Cell Reports, Volume *30*

Supplemental Information

Neuronal BIN1 Regulates Presynaptic Neurotransmitter Release and Memory Consolidation

Pierre De Rossi, Toshihiro Nomura, Robert J. Andrew, Nicolas Y. Masse, Vandana Sampathkumar, Timothy F. Musial, Ari Sudwarts, Aleksandra J. Recupero, Thomas Le Metayer, Mitchell T. Hansen, Ha-Na Shim, Sofia V. Krause, David J. Freedman, Vytas P. Bindokas, Narayanan Kasthuri, Daniel A. Nicholson, Anis Contractor, and Gopal Thinakaran

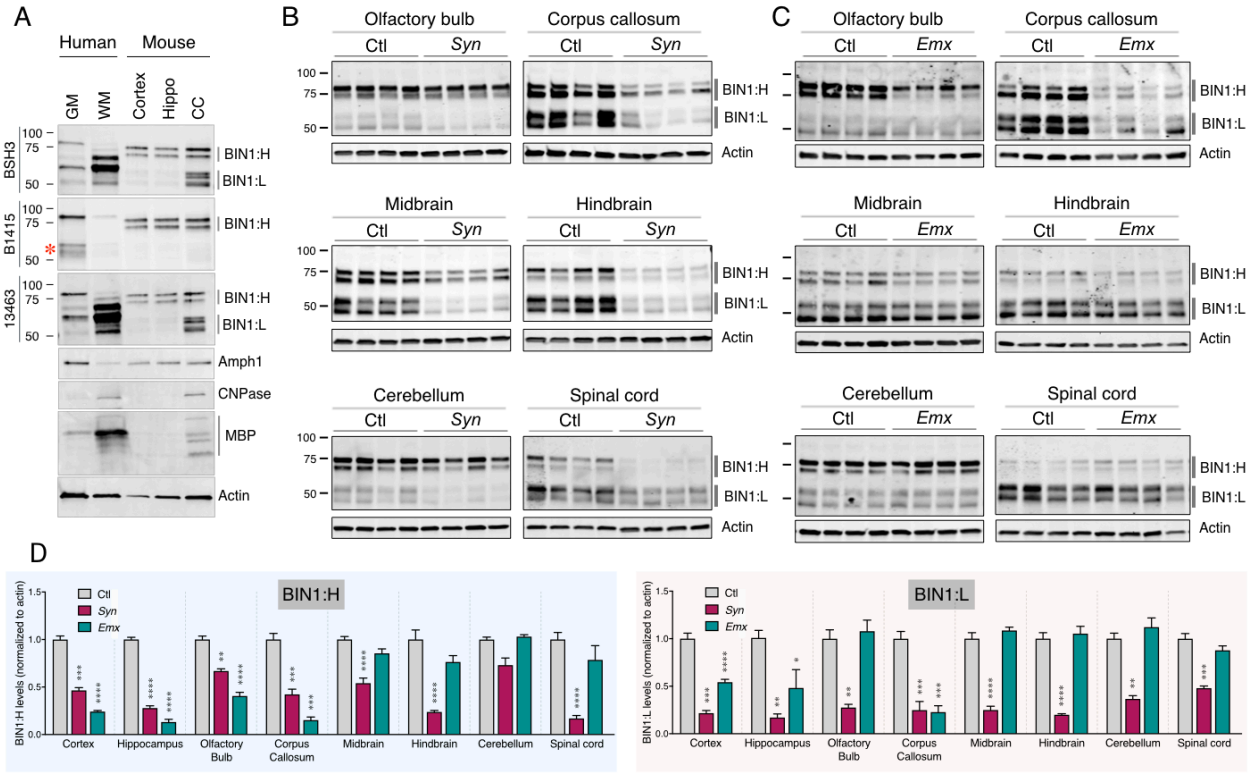

Figure S1. Related to Figure 1: **Analysis of BIN1 expression in brain.**

(A) A comparison of BIN1 expression in human and mouse brain. Antibodies BSH3 and 13463 are capable of detecting all BIN1 isoforms, whereas pAb B1415, raised against the CLAP domain, can only recognize the BIN1 isoforms containing the CLAP domain (BIN1:H). Only low levels of BIN1:H isoforms were detected in the grey matter in the human brain, whereas they are relatively more abundant in the mouse brain. The isoforms lacking the CLAP domain (BIN1:L) are abundant in the human brain white matter and mouse brain corpus callosum. Amph1 (neurons) and CNPase and MBP (oligodendrocytes) were used as markers. An *asterisk* indicates a non-specific signal observed in human brain gray matter.

(B) Microdissection analysis of BIN1 levels in the central nervous system regions of *Syn* mice and littermates. BIN1 was detected using pAb 14647 (detects all BIN1 isoforms), and actin was used as the loading control.

(C) Microdissection analysis of *Emx* mice and littermates.

(D) Quantification of relative BIN1:H and BIN1:L isoforms normalized to actin. The mean ± SEM are plotted in each graph. *p<0.05, **p<0.01, ***p<0.001, ****p<0.0001.

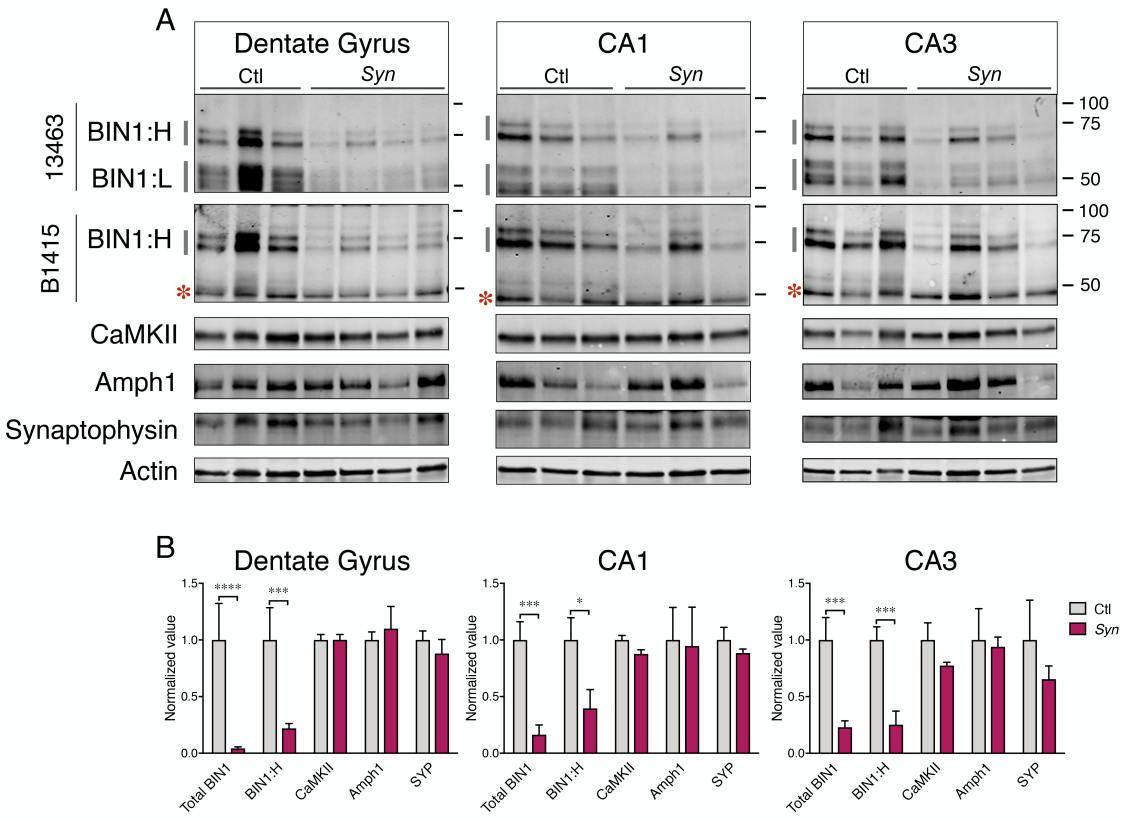

Figure S2. Related to Figure 1: **Microdissection analysis of BIN1 levels in the hippocampus of Ctl and *Syn* mice.**

(A) Western blot analysis of BIN1 and neuronal marker levels in the dentate gyrus (left), CA1 (middle), and CA3 (right) regions. BIN1 was analyzed using antibodies 13463 and B1415. Red *asterisks* indicate a non-specific protein detected by antibody B1415. The levels of CaMKII, Amph1, and synaptophysin were also quantified.

(B) Quantification of relative protein levels normalized to actin. The levels of BIN1 were significantly reduced in *Syn* mice, but the levels of CaMKII, synaptophysin, and Amph1 were not altered in cKO mice.

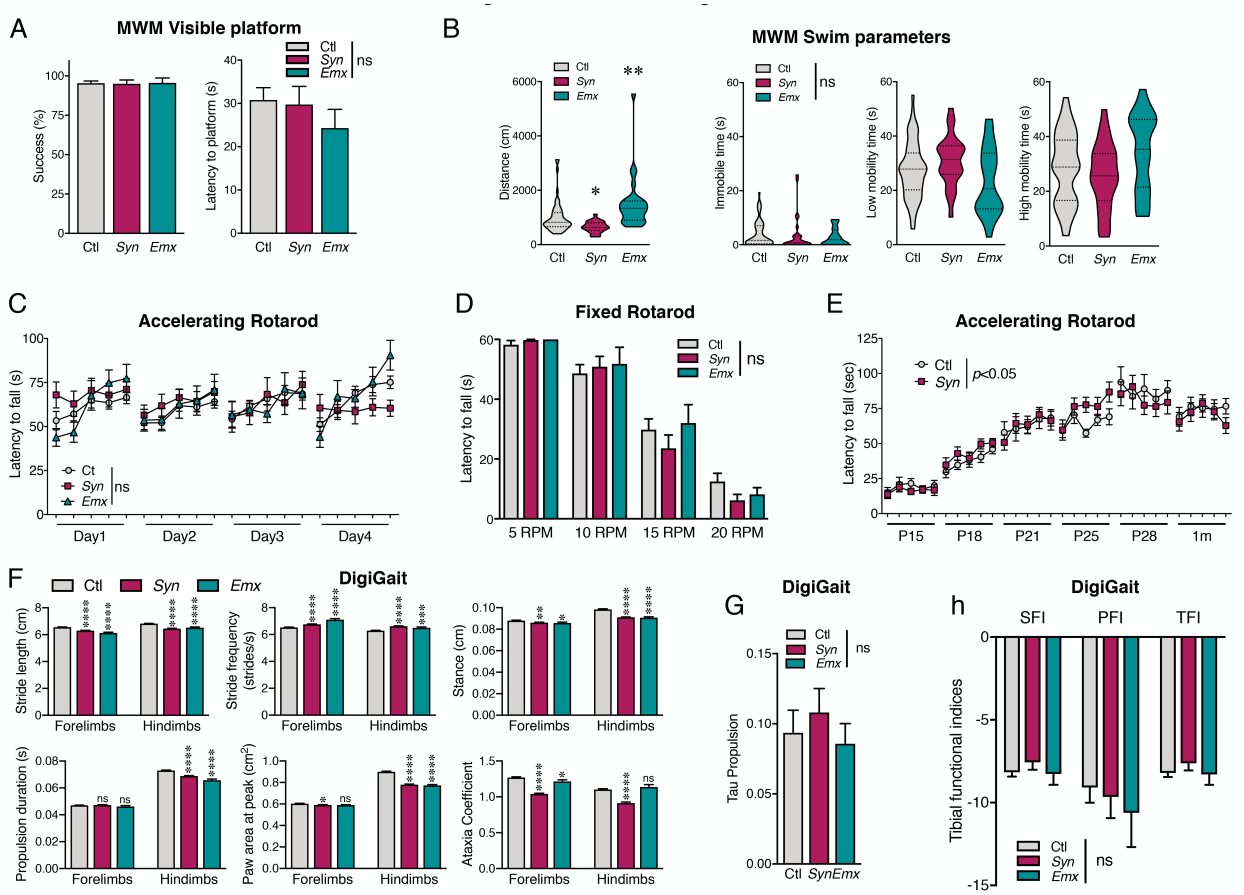

Figure S3. Related to Figure 2: **Neuronal knock-out of *Bin1* does not induce physical impairments.**

(A) Graphs representing performances (success and time to escape) recorded during Morris water maze visible platform test (see fig1e). The mean ± SEM are plotted. No significant difference was observed between the groups by ANOVA. Success: $F_{(2,104)}$=0.01446, p=0.9856; latency: $F_{(2,104)}$=0.8371, p=0.4358; n=52 Ctl, 28 *Syn* and 27 *Emx*).

(B) Violin plots depict the distribution of swimming distance and mobility in the probe trial. Swimming parameters during the probe trial, analyzed by ANOVA, revealed significant differences between the Ctl and cKO groups in the swim distance ($F_{(2, 106)}$=11.99, p<0.0001). There were also significant differences in the duration of low-mobility ($F_{(2, 106)}$=3.738, p=0.027) and duration of high-mobility ($F_{(2, 106)}$=30127, p=0.0479), but Tukey's post-hoc analysis revealed that the significance existed only between the two cKO groups and not the Ctl group.

(C) The line graph represents the performance (latency to fall) of 6 weeks-old mice on the accelerating rotarod (mean ± SEM). No significant difference between the groups was observed ($F_{(2, 68)}$=0.166, p=0.847, n=39 Ctl, 19 *Syn*, and 13 *Emx*).

(D) The graph represents performance (latency to fall) of 6 weeks-old mice on the fixed rotarod (mean ± SEM). No significant difference between the groups was observed ($F_{(2, 68)}$=0.303, p=0.74, n=39 Ctl, 19 *Syn*, and 13 *Emx*).

(E) The line graph represents the performance of a cohort of *Syn* mice on the accelerating rotarod (mean ± SEM) during postnatal development. A small but significant difference between the groups was observed ($F_{(1, 993)}$=5.135, p=0.024; n=18 Ctl and 19 *Syn*).

(F) Significant differences between the groups were observed on multiple parameters recorded by DigiGait (stride length and frequency, stance, propulsion duration, paw area at peak, and ataxia coefficient) in 1.5-month-old mice are plotted (mean ± SEM). However, these differences were too small to impact on the animals' general mobility.
(G) The graph represents the Tau propulsion (mean ± SEM). No difference between the groups was recorded (ANOVA, $F_{(2, 94)}$=0.3009, p=0.7409).
(H) The graph represents sciatic, peroneal, and posterior tibial nerve parameters (Bain et al., 1989) recorded using DigiGait analysis (mean ± SEM). No difference between the groups was recorded (ANOVA, $F_{(2, 282)}$=0.4422, p=0.6430).

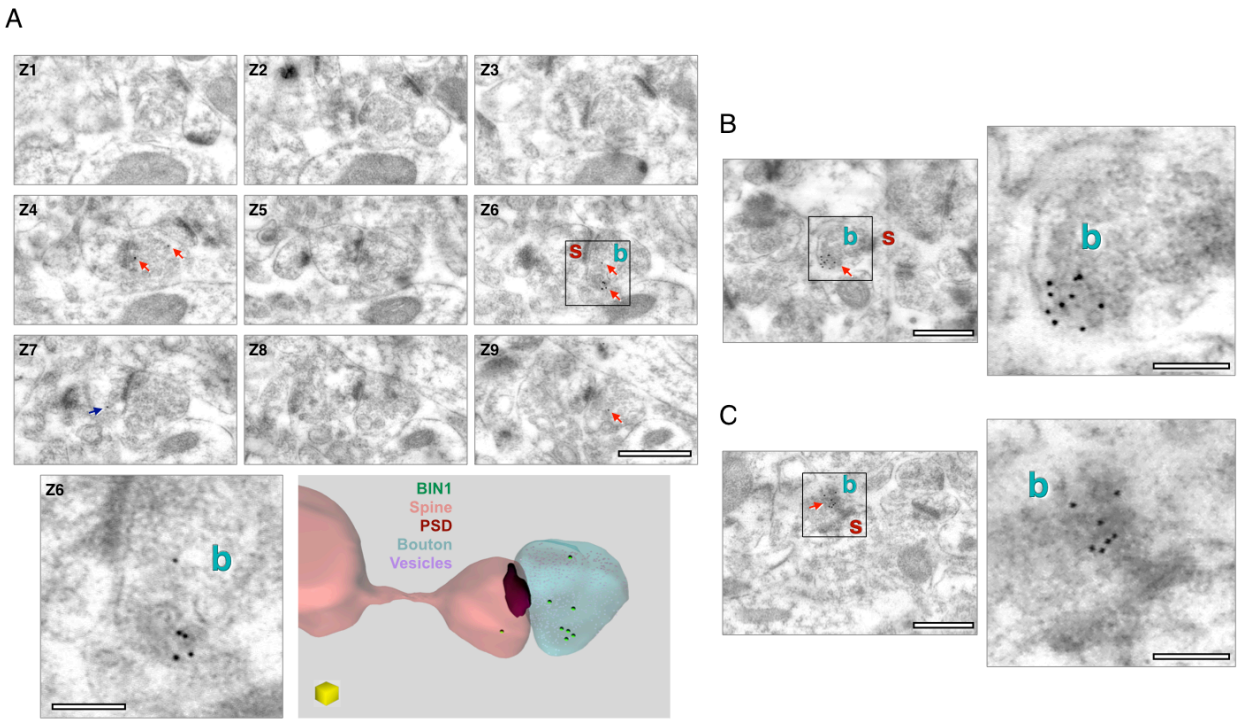

Figure S4. Related to Figure 5: **Presynaptic enrichment of BIN1.**

(A) Micrographs of nine serial sections through an axospinous synapse in CA1 *stratum radiatum* (Z1-Z9) illustrating that BIN1 can be detected at both pre- and postsynaptic sites. Note that BIN1 immunogold localization in the presynaptic axonal bouton (*b*) is considerably higher than that in the postsynaptic dendritic spine (*s*). Eight immunogold particles for BIN1 can be seen in the presynaptic terminal (red arrows), as compared to one in the postsynaptic dendritic spine (blue arrow). The boxed region of the presynaptic terminal in Z6 is shown at a higher magnification at the bottom (left). At the bottom right is a 3-dimensional reconstruction of the synapse and BIN1 immunogold particles as visualized in Z1-Z9.

(B and C) Two more examples of presynaptic localization of BIN1, captured in micrographs of single sections through a small non-perforated synapse (top) and a larger perforated synapse (bottom). Panels on the right are higher magnification images of the regions marked by the boxes.

Scale bars main images: 500 nm; higher magnification images: 150 nm.

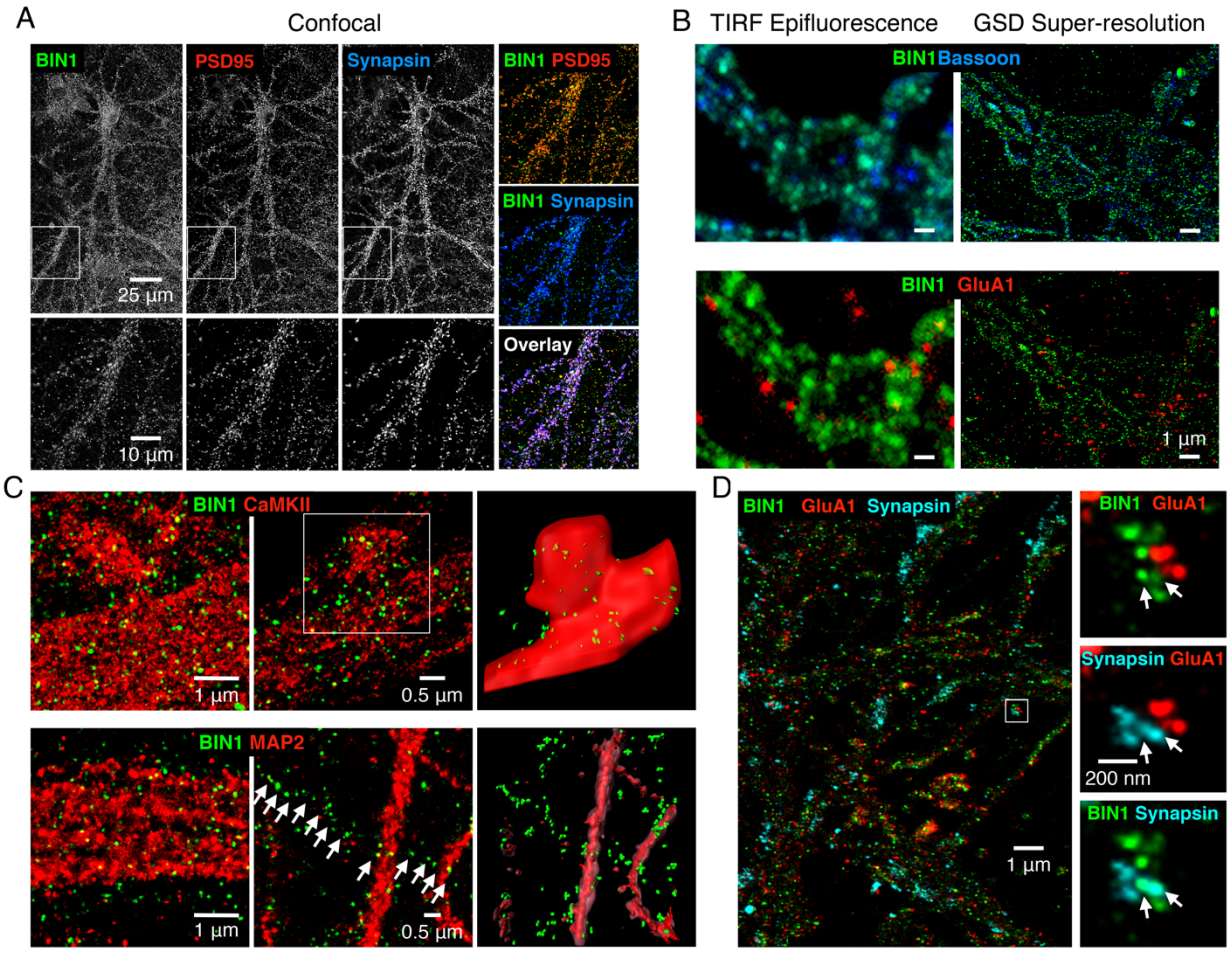

Figure S5. Related to Figure 5: **Super-resolution analysis of BIN1 presynaptic localization.**

(A) Representative confocal images for BIN1 along with synapsin (presynaptic marker), and PSD95 (postsynaptic marker). The overlays show a high level of colocalization between BIN1 and synaptic markers.

(B) The gain of resolution obtained using dSTORM microscopy for BIN1 (green) as well as synaptic proteins Bassoon (blue) and GluA1 (red).

(C) Top: localization of BIN1 (green) within CaMKII-positive structures (red). Imaris reconstruction (right panel) shows a low frequency of BIN1 signal within the spines. Bottom: localization of BIN1 (green) in MAP2-positive dendrites (red). A lower incidence of BIN1 staining was observed in the dendritic shaft. BIN1 puncta were found in MAP2-negative structures (white arrows), highlighted by filament tracing in Imaris (right panel).

(D) dSTORM analysis of BIN1 colocalization with pre- and postsynaptic markers. The boxed region is shown at a higher magnification on the right as two-color overlays. *White arrows* indicate the overlap between BIN1 and synapsin.

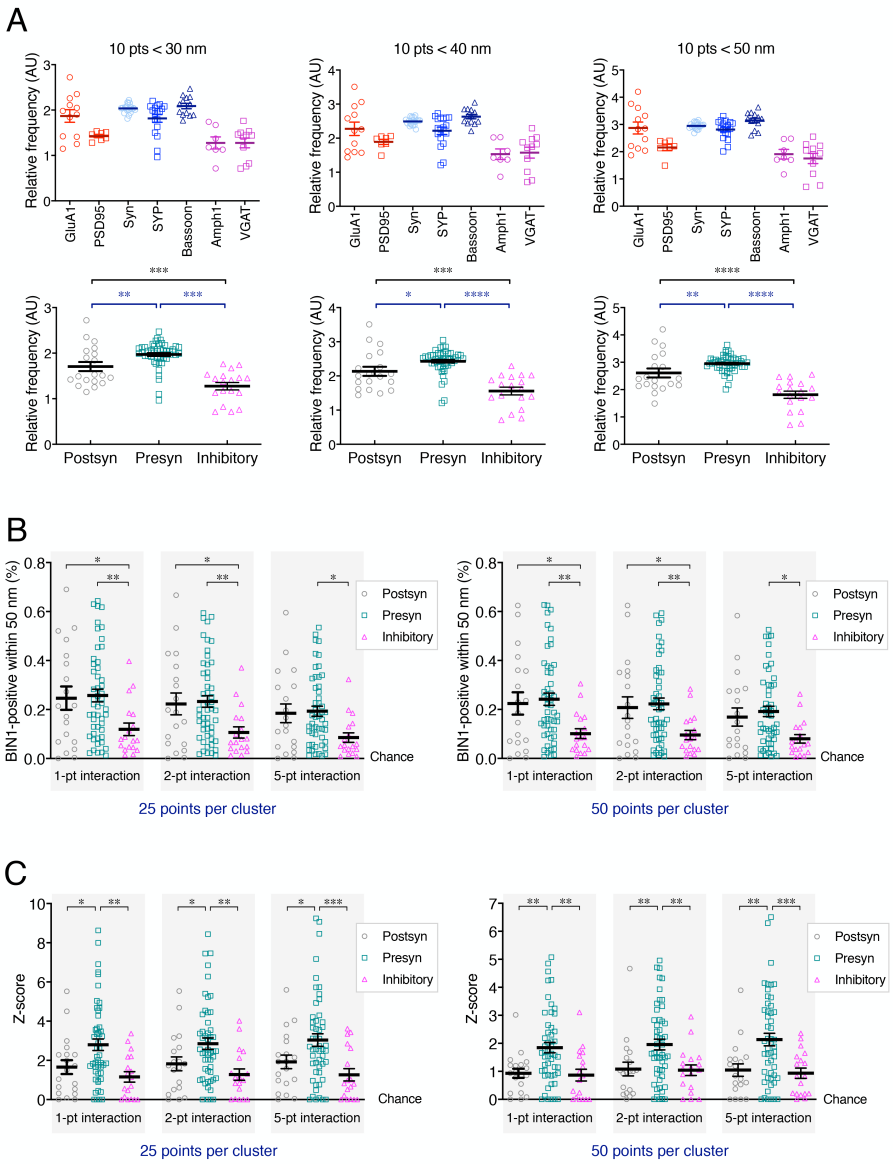

Figure S6. Related to Figure 5: **Quantification of the distance between BIN1 and different synaptic markers.**

(A) DBSCAN analysis of cluster proximity showing proportion of BIN1 within 30 nm, 40 nm, and 50 nm of each synaptic marker (top graphs) or grouped postsynaptic, presynaptic, and inhibitory presynaptic markers (bottom graphs). Note that the top graphs in panel A are color coded differently from the rest of the graphs.

(B) Graph representing the proportion of BIN1-positive structures within 50 nm of synaptic markers. BIN1 was found associated more with general presynaptic sites (25-pt clustering $F_{(8, 255)}$=3.819, p=0.0003; 50-pt clustering $F_{(8, 255)}$=3.784, p=0.0003).

(C) Graph representing randomization analysis of BIN1 proximity to synaptic markers. When the Z score is equal to 0, the association between BIN1 and the markers is not greater than chance The results of the Z score analysis showed specific association of BIN1 with the different markers analyzed (25-pt clustering $F_{(8, 255)}$=4.706, p<0.0001; 50-pt clustering $F_{(8, 255)}$=5.446, p<0.0001).

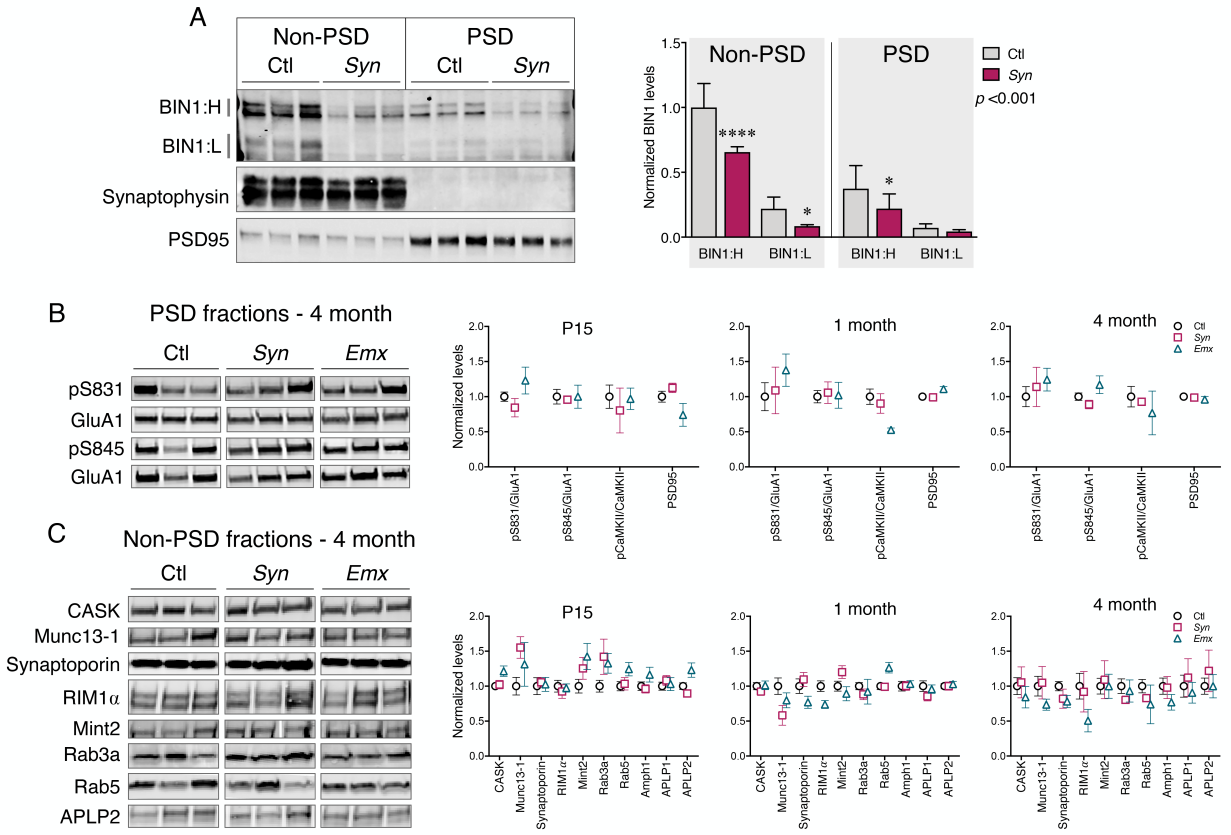

Figure S7. Related to Figures 5 and 7: **Synaptosome fractionation analysis of synaptic protein levels in *Bin1* cKO mice.**

(A) Western blot analysis of non-PSD and PSD fractions of hippocampus tissue from Ctl and *Syn* mice. The blots were probed with antibodies against BIN1 (mAb 13463), synaptophysin and PSD95. The graph (right) represents quantification of BIN1 levels in each fraction normalized to BIN1 in Ctl non-PSD fractions.

(B) The levels of GluA1 phosphorylation in PSD fractions of Ctl, *Syn*, and *Emx* mice analyzed at 4 months of age. The graphs on the right represent the ratio of p831/GluA1, p845/GluA1, and pCaMKII/CaMKII, and PSD95 levels [normalized to Ctl mice] in mice analyzed at P15 ($F_{(6, 101)}$= 0.8136, p=0.5618), 1 month ($F_{(6, 55)}$=1.428, p=0.2208) and 4 months of age ($F_{(6, 76)}$=0.7103, p=0.6423).

(C) The levels of CASK, Munc13-1, Synaptoporin, RIM1, Mint2, Rab3a, Rab5 and APLP2 in the non-PSD fraction in Ctl, *Syn*, and *Emx* mice at 4 months of age. On the right, graph representing level of presynaptic proteins at P15 (left) ($F_{(18, 230)}$=1.397, p=0.1338), 1 month (middle) ($F_{(18, 140)}$=2.109, p=0.0116) and 4 months of age (right) ($F_{(18, 150)}$=0.4135, p=0.9835).

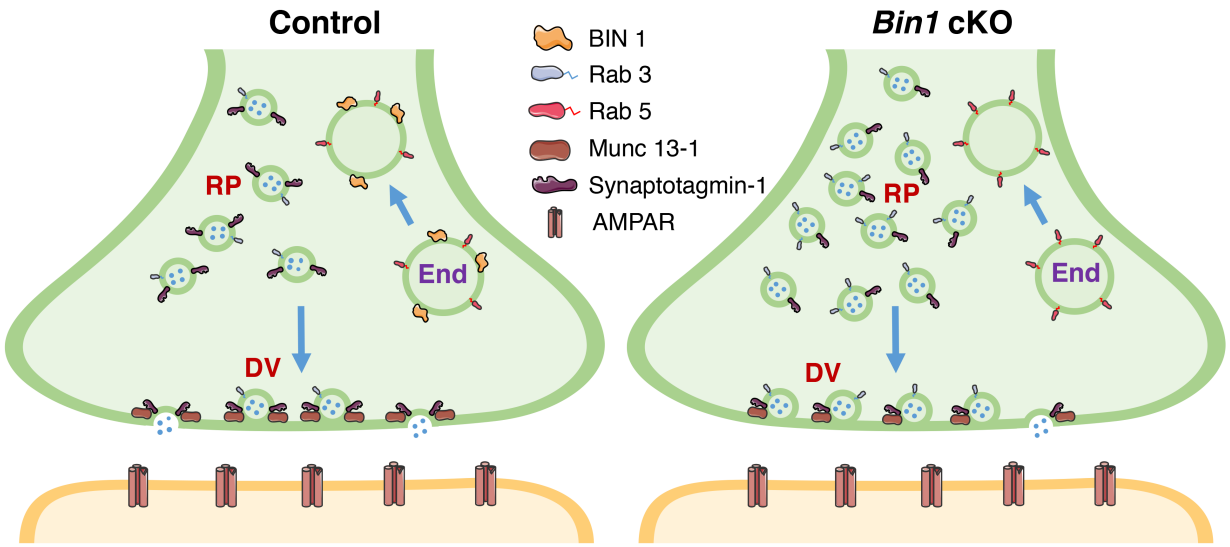

Figure S8. Related to Figures 7 and 8: **Schematic representation of presynaptic changes *Bin1* cKO mice.** Our results suggest that BIN1 localizes to the synapse and participates in synaptic vesicle dynamics in glutamatergic neurons. In the absence of BIN1, excitatory synapses onto hippocampal CA1 pyramidal neurons have increased number of docked synaptic vesicles (*DV*) concomitant with a significant reduction in presynaptic vesicular release probability. The decrease in the cluster organization of SNARE-related presynaptic proteins may underlie this defect. The loss of BIN1 also leads to an increase in reserve pool of synaptic vesicles (*RP*), consistent with a slower depletion time course of synaptic responses. In addition, the loss of BIN1 leads to an increase in the size of Rab5 clusters in *Bin1* cKO mice, in agreement with the data from cultured neurons (Calafate et al., 2016). We propose that the altered synaptic vesicle dynamics in *Bin1* cKO mice reflects a critical role of BIN1 in the regulation of exocytosis associated with synaptic transmission in addition to its previously described role in endocytosis. *End*, endosome.

Table S1. List of antibodies used in this study, Related to STAR Methods

Target	Species / clone	Catalog no.	Source	WB	IF
BIN1	mAb EPR13463	ab182562	AbCam	1:500	1:200
BIN1	Rabbit pAb	14647-1-AP	Protein Tech	1:500	
BIN1	Rabbit pAb BSH3		Thinakaran Lab	1:1000	1:2500
BIN1	Rabbit pAb B1415		Thinakaran Lab	1:2000	
Actin	mAb 2D4H5	66009-I-Ig	Protein Tech	1:20000	
AmphI	mAb 8	SC21710	Santa Cruz	1:2000	1:1000
APLP1	Rabbit pAb CT11		Thinakaran Lab	1:1000	
APLP2	Rabbit pAb CT12		Thinakaran Lab	1:1000	
Bassoon	Guinea Pig pAb	141-004	Synaptic Systems		1:500
CaMKII	mAb 6G9	SC32288	Santa Cruz	1:500	
CASK	mAb K56A/50	O14936	NeuroMab	1:1000	
CNPase	mAb 11-5B	MAB326	Millipore	1:2000	
Flotillin-2	Rabbit pAb		Thinakaran Lab	1:1000	
GluA1	mAb N355/1	P19490	NeuroMab	1:100	1:50
MAP2	mAb HM-2	M4403	Sigma		1:10000
MBP	mAb SMI-94	SMI-94R	Covance	1:20000	
Mint-2	mAb	M76120	BD Biosciences	1:500	
Munc13-1	Rabbit pAb	126-102	Synaptic Systems	1:1000	1:500
NeuN	mAb A60	MAB377	Chemicon		1:2000
pCaMKII	Rb mAb D21E4	12716S	Cell Signaling	1:2000	1:500
pGluA1-831	Rabbit pAb	AB5847	Millipore	1:500	
pGluA1-845	Rabbit pAb	AB5849	Millipore	1:500	
PSD95	mAb K28/43	K28/43	UC Davis	1:5000	
Rab3a	mAb (Clone9)	Sc-136050	Santa Cruz	1:500	1:100
Rab5	Rb mAb C8B1	3547S	Cell Signaling	1:1000	1:500
RIM1α	Rabbit pAb	140-003	Synaptic Systems	1:1000	1:500
Synapsin 1	mAb 46.1	106 011BT	Synaptic Systems		1:5000
Synaptojanin 1	Rabbit pAb	145-103	Synaptic Systems		1:200
Synaptophysin 1	mAb SVP38	S5768	Sigma	1:20000	1:500
Synaptoporin	Rabbit pAb	102-003	Synaptic Systems	1:1000	1:500
Synaptotagmin 1	Chicken IgY	105-106	Synaptic Systems		1:300

Table S2. Statistical analysis of cluster density quantified by confocal imaging, Related to Figure 1

Protein	ANOVA F (DFn, DFd)	Ctl vs *Syn*	Ctl vs *Emx*
BIN1	F (2, 107) = 50.70, $p < 0.0001$	<0.0001	<0.0001
RIM1	F (2, 28) = 0.2967, $p = 0.7456$	0.6426	0.4507
Munc13-1	F (2, 26) = 2.935, $p = 0.0709$	0.5138	0.0247
Bassoon	F (2, 152) = 6.403, $p = 0.0021$	0.0014	0.0058
Synapsin1	F (2, 95) = 0.5160, $p = 0.5986$	0.4142	0.8883
Synaptojanin	F (2, 29) = 0.8146, $p = 0.4527$	0.3184	0.2612
Synaptoporin	F (2, 31) = 4.054, $p = 0.0273$	0.0162	0.0258
Synaptotagmin	F (2, 66) = 1.101, $p = 0.3385$	0.1884	0.2269
GluA1	F (2, 69) = 2.330, $p = 0.1049$	0.1644	0.0398
pCaMKII	F (2, 29) = 3.010, $p = 0.0649$	0.0288	0.7094
PSD95	F (2, 93) = 0.4385, $p = 0.6463$	0.4927	0.3887
Rab5	F (2, 128) = 7.376, $p = 0.0009$	0.0004	0.0060
Rab3a	F (2, 61) = 0.3307, $p = 0.7197$	0.5214	0.4664
Clathrin	F (2, 30) = 1.209, $p = 0.3127$	0.1589	0.2464
Dynamin	F (2, 30) = 30632, $p = 0.0387$	0.0168	0.0547

The table reports statistical analysis of data from a minimum of 7 images from at least 3 animals per genotype. ANOVA F statistic, degrees of freedom between groups (DFn) and within groups (DFd), and the *p* value are listed. The right two columns list the *p* value of post-hoc Fisher's LSD after ANOVA for Ctl *versus* each *Syn* or *Emx* mice.

Table S3. Statistical analysis of cluster volume quantified by STED imaging, Related to Figure 7

Protein	ANOVA F (DFn, DFd)	Ctl vs *Syn*	Ctl vs *Emx*
BIN1	F (2, 8298) = 31.61, $p < 0.0001$	<0.0001	0.0706
Rab5	F (2, 47322) = 60.44, $p < 0.0001$	0.0018	<0.0001
Rab3a	F (2, 25397) = 50.55, $p < 0.0001$	<0.0001	<0.0001
Synaptotagmin-1	F (2, 84385) = 145.8, $p < 0.0001$	<0.0001	<0.0001
Munc13-1	F (2, 8375) = 14.60, $p < 0.0001$	<0.0001	0.0021
Synaptophysin	F (2, 3695) = 8.192, $p = 0.0003$	0.0011	0.0001
Synaptoporin	F (2, 7953) = 39.13, $p < 0.0001$	<0.0001	<0.0001
Bassoon	F (2, 19454) = 18.41, $p < 0.0001$	0.9496	<0.0001
Synaptojanin	F (2, 4914) = 52.24, $p < 0.0001$	<0.0001	0.2331
RIM1	F (2, 17957) = 1.475, $p = 0.2289$	0.0891	0.2457
Synapsin1	F (2, 39891) = 3.562, $p = 0.0284$	0.0638	0.3574
GluA1	F (2, 17662) = 249.5, $p < 0.0001$	0.1483	<0.0001
pCaMKII	F (2, 7224) = 64.07, $p < 0.0001$	<0.0001	<0.0001
PSD95	F (2, 6966) = 1.058, $p = 0.3471$	0.1811	0.2759

The table reports statistical analysis of data from a minimum of 6 images from at least 3 animals per genotype. ANOVA F statistic, degrees of freedom between groups (DFn) and within groups (DFd), and the *p* value are listed. The right two columns list the *p* value of post-hoc Fisher's LSD after ANOVA for Ctl *versus* each *Syn* or *Emx* mice.